Atomic Spectroscopy

Article

Thiol-functionalized Fe_3O_4-modified Membrane for Selective Preconcentration and Sensitive Detection of Metallic Copper Nanoparticles in Environmental Waters

Xinyuan Huang, Jia Lv, Siyuan Wang, Wanying Li, and Ke Huang *

College of Chemistry and Material Science, Sichuan Normal University, Chengdu 610068, P. R. China

Received: *September 28, 2025;* ***Revised:*** *October 30, 2025;* ***Accepted:*** *October 31, 2025;* ***Available online:*** *October 31, 2025.*

DOI: 10.46770/AS.2025.158

ABSTRACT: Membrane filtration is an efficient technique for rapid and precise separation, yet challenges persist in distinguishing and selectively separating nanoparticles with identical elemental compositions, especially copper-based nanoparticles. Here, we report for the first time the immobilization of thiol-functionalized Fe_3O_4 nanoparticles (Fe_3O_4 – RSH NPs) onto mixed cellulose ester membranes for the selective separation and preconcentration of copper nanoparticles (Cu NPs). The Fe_3O_4–RSH NPs–modified membrane demonstrated significantly greater retention of Cu NPs than CuS and CuO NPs of comparable size. The functionalized membrane exhibits exceptional separation performance, achieving over 90% retention of Cu NPs and an enrichment factor of ~23, as verified by inductively coupled plasma mass spectrometry (ICP-MS). Notably, the retention rate of Cu NPs remained unaffected by other copper species, demonstrating the excellent selectivity of the modified membrane toward Cu NPs. Under optimized conditions, the method reached a limit of detection (LOD) of 2.2 pg mL^{-1} for Cu NPs. Furthermore, the approach enabled successful detection of Cu NPs in river water samples from Chengdu. This strategy provides a rapid, reliable, and cost-effective pretreatment method for trace nanoparticle analysis in environmental samples and offers a promising platform for the development of low-cost, on-site nanoparticle monitoring technologies.

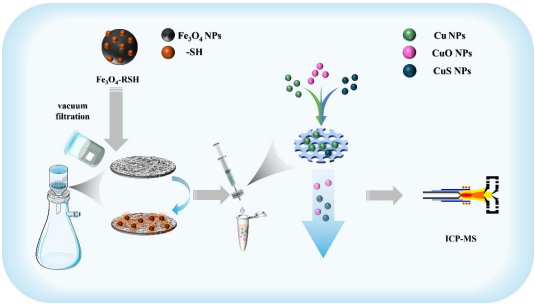

INTRODUCTION

Copper-based nanoparticles comprise a diverse group of materials, such as copper nanoparticles (Cu NPs), copper sulfide nanoparticles (CuS NPs), and copper oxide nanoparticles (CuO NPs).[1,2] Owing to their distinctive physicochemical properties, these materials have found extensive applications in catalysis, environmental remediation, and biomedicine.[3] However, their widespread use has raised growing concerns about potential environmental and biological risks.[4] The toxicity of copper-based NPs is strongly influenced by their chemical composition and particle size, with Cu NPs exhibiting toxicological behaviors distinct from those of CuS and CuO NPs.[5 6] Understanding these differences is critical for accurately assessing the ecological impacts associated with their environmental release.[7, 8] Therefore, developing analytical strategies capable of selectively separating and preconcentrating trace Cu NPs from complex environmental matrices is essential for enhancing the precision of environmental monitoring and risk evaluation.

Various methods are employed for the separation of nanoparticles, including cloud point extraction (CPE), ultracentrifugation, dialysis, chromatography, and dielectrophoresis.[9-13] Current research has predominantly focused on the separation of Au NPs, Ag NPs, and their corresponding ions, while comparatively fewer studies have addressed the separation and detection of copper-based nanoparticles due to their similar physicochemical properties.[14,15] Moreover, existing methods for detecting Cu NPs primarily rely on single-particle ICP-MS,[16] cloud-point extraction to CPE,[17] and combined spectroscopic

techniques such as X-ray absorption near-edge structure (XANES) and extended X-ray absorption fine structure (EXAFS).[18] Although these methods exhibit good analytical performance, several limitations remain. For example, SP-ICP-MS cannot effectively distinguish Cu NPs smaller than 20 nm, CPE involves complex and time-consuming procedures, and XANES/EXAFS instrumentation is prohibitively expensive. Consequently, there is still a lack of a rapid, cost-effective, and efficient method for the separation and analysis of Cu NPs. Membrane filtration technology is widely valued for its operational simplicity, high efficiency, and cost-effectiveness.[19] It enables rapid and reliable separations, making it an indispensable tool for the pretreatment of environmental samples.[20,21] However, conventional unmodified membranes primarily rely on size-exclusion mechanisms, which severely limit their ability to distinguish nanoparticles with similar sizes and elemental compositions.[22] This limitation highlights the importance of enhancing membrane selectivity through surface functionalization.[23, 24]

Recent advancements have demonstrated that modifying filter membranes with specific materials, such as functional groups, nanoparticles, or polymer coatings, can substantially improve their selectivity and efficiency in separation.[25,26] Fe_3O_4 nanoparticles are effective separation materials owing to their superparamagnetic properties, which enable their use as magnetic fluids for efficient separation processes.[27] Moreover, Fe_3O_4 NPs themselves exhibit exceptional performance in material separation due to their high specific surface area, which increases the number of active sites available for surface modification.[28] This characteristic is particularly advantageous for capturing target substances, making Fe_3O_4 NPs highly effective in adsorbing trace analytes.[29] Additionally, Fe_3O_4 NPs possess multiple surface functional groups that serve as reactive sites, providing abundant opportunities for membrane modification and interaction.[30] Functionalization with specific ligands can greatly enhance the separation performance of Fe_3O_4 NPs toward their target analytes. For example, Li *et al.* successfully extracted and detected trace levels of methylmercury and ethylmercury in aqueous media using thiol-modified magnetic mesoporous Fe_3O_4 NPs [31]. Similarly, Qurat et al. reported a composite material incorporating PDA-modified Fe_3O_4 NPs onto bentonite, which effectively adsorbed dyes such as crystal violet.[32] Owing to their excellent selective adsorption and hydrophilic properties, Fe_3O_4 NPs can enhance the performance of filter membranes when used for surface modification. In particular, incorporating functionalized nanoparticles, such as thiol-modified Fe_3O_4 NPs, can significantly improve the membrane's selectivity for separating target nanoparticles.[33] This offers a promising approach for selectively isolating copper-based nanoparticles from complex environmental samples.

In this study, a novel Fe_3O_4–RSH nanoparticle-modified mixed cellulose ester (MCE) membrane was developed for the first time to enable the selective separation and preconcentration of Cu NPs from mixtures containing CuO and CuS NPs of comparable sizes (Scheme. 1). The modified membrane demonstrated excellent separation performance, achieving retention rates exceeding 90% and an enrichment factor of approximately 23, as confirmed by ICP–MS analysis of the filtrate. Mechanistic investigations revealed that the high selectivity arises from the synergistic effects of the Donnan potential and the specific interaction between sulfhydryl groups and Cu NPs. This work represents the first successful application of a surface-modified filter membrane for the efficient and selective separation of Cu NPs, enabling accurate trace-level detection in complex matrices. The proposed strategy not only expands the range of nanoparticle separation methodologies but also provides a rapid, cost-effective, and highly selective pretreatment approach for trace nanoparticle analysis in environmental monitoring.

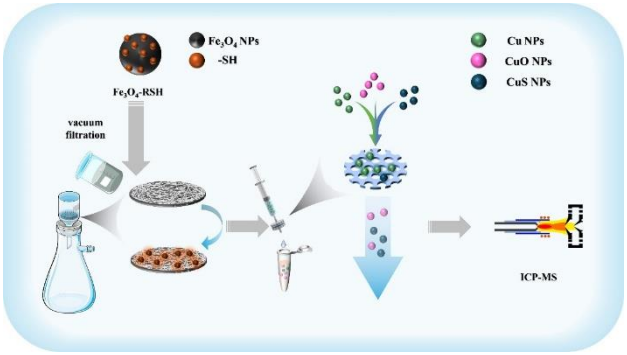

Scheme. 1 Schematic illustration of the preparation and filtration process of Fe_3O_4-RSH NPs modified membranes.

EXPERIMENTAL

Reagents and materials. Mixed cellulose membranes (pore size: 0.22 μm / 0.45 μm, diameter: 50 mm) and Nylon 66 membranes (pore size: 0.22 μm / 0.45 μm, diameter: 50 mm) were procured from Chengdu Feierste Instrument Co., Ltd. $FeCl_3·6H_2O$, $FeCl_2·4H_2O$, and TEOS (95%) were sourced from Shanghai Macklin Biochemical Co., Ltd. 3-MPTMS, Au NPs (5 nm), Ag NPs (5 nm) were procured from Shanghai Aladdin Biochemical Technologies Co., Ltd. Ethanol (99.7%), methanol (99.9%), NaOH (98.0%), and ammonia solution were purchased from Chengdu Kelong Chemicals Co., Ltd. Cu NPs (5 nm, 20 nm and 100 nm) and CuO NPs (5 nm) solutions were sourced from Beijing Zhongke Keyou Technology Co., Ltd. All chemicals were used as received, without any pretreatment. Deionized water (18.25 MΩ cm^{-1}) for the experiments was supplied by an ultrapure water system from Chengdu Ultrapure Water Technology Co., Ltd., China. All reagents used were of analytical grade or higher purity.

Fabrication of Fe_3O_4 NPs-modified filtration membranes. Fe_3O_4-RSH NPs were synthesized according to the previous method outlined in the Supporting Information.[31] As illustrated in Scheme 1, the filtration modified with Fe_3O_4-RSH NPs was fabricated on a hydrophilic MCE membrane (0.22 μm pore size) using vacuum filtration. Initially, 0.02 g of Fe_3O_4-RSH NPs was weighed and dispersed in 500 mL of distilled water, followed by shaking and ultrasonic treatment for 10 min. The resulting suspension was subsequently vacuum-filtered through the MCE membrane. After filtration, the membrane was rinsed twice with distilled water using a wash bottle to remove any residual impurities. The modified composite membrane was then air-dried at room temperature.

Characterization of Membranes. The surface morphology of the membranes was examined using a scanning electron microscope (SEM, ZEISS Sigma 360, Germany) at an accelerating voltage of 15 kV. The surface chemical composition of the materials and membrane samples was analyzed by a X-ray photoelectron spectroscopy (XPS, K-Alpha™, Thermo, USA) with an Al Kα X-ray source. Fourier-transform infrared spectroscopy (FTIR, VERTEX 70 spectrometer, Bruker, Germany) was used to characterize the functional groups on the membrane surface. The crystal structure and phase composition of the modified material were tested using an X-ray diffractometer (XRD). The zeta potentials of different types of copper-based nanoparticles and thiol-functionalized Fe_3O_4 NPs were measured using a Zeta potential analyzer (Nano ZSP, Malvern, UK). Filtration performance was evaluated using ICP-MS (Agilent 8900, USA).

For the ICP-MS analysis, the Fe_3O_4-RSH NPs - modified filtration were placed in a filtration holder. Copper-based NPs solution (Cu NPs, CuS NPs, and CuO NPs) was filtered through a syringe filter. The concentration of copper in the feed solution and filtrate was determined using ICP-MS to evaluate the filtration performance. The rejection rate was calculated using the following equation:

$$\text{Rejection ratio (\%)} = \frac{C_0 - C_1}{C_0} \quad (1)$$

where C_0 is the concentration of Cu NPs in the feed solution, and C_1 is the concentration in the filtrate. Error bars represent the standard deviation from at least three parallel measurements.

Sample Analysis. Water samples were collected from four different lakes in Chengdu. Cu NPs were added to 25 mL of environmental water samples and filtered. Subsequently, Cu NPs on the filter membrane were eluted from the filter membrane using 1 mL of nitric acid (2%, v/v), followed by ultrasonication and phase separation. The ultrasonicated solution were analyzed using ICP-MS.

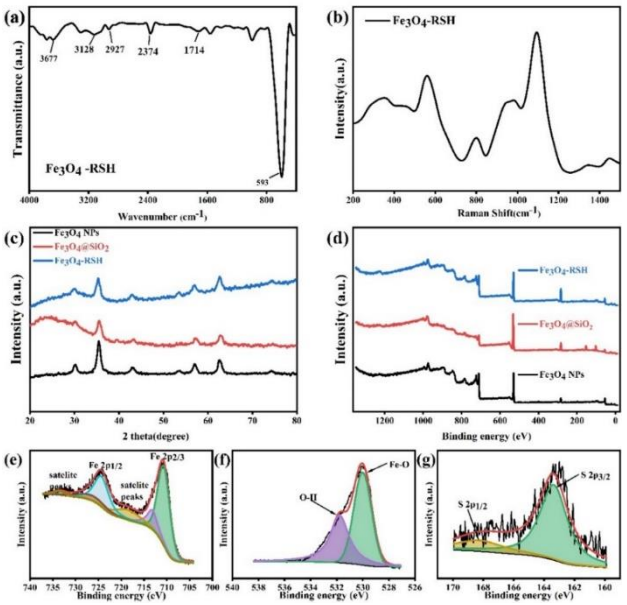

Fig. 1 (a) FTIR spectra of Fe_3O_4-RSH NPs. (b) SERS spectrum of Fe_3O_4-RSH NPs. (c) XRD patterns of three types of Fe_3O_4 NPs. (d) XPS spectra of three types of Fe_3O_4 NPs. (e) Peak distribution in XPS spectrum of element Fe. (f) Peak distribution in XPS spectrum of element O. (g) Peak distribution in XPS spectrum of element S.

RESULTS AND DISCUSSION

Characterization of Fe_3O_4-RSH NPs and copper-based nanoparticles. As shown in Fig. S1, SEM images reveal that Fe_3O_4 NPs, Fe_3O_4-RSH NPs, and Fe_3O_4@SiO_2 NPs are randomly dispersed. Notably, Fe_3O_4 NPs have a strong tendency to aggregate, mainly as a result of intrinsic magnetic dipole interactions and surface energy–driven orientation effects.[34] Fig. 1a shows the FTIR spectrum of Fe_3O_4–RSH NPs. The characteristic absorption bands at 1714 and 593 cm^{-1} are assigned to Fe–O bond vibrations, while the peak at 2927 cm^{-1} is attributed to trace CH_2 groups introduced by 3-MPTMS during synthesis.[35] A weak absorption band associated with the S–H bond is observed at 2374 cm^{-1}, which can be ascribed to the sulfur of the thiol groups in Fe_3O_4–RSH NPs. In comparison with Fe_3O_4 NPs and Fe_3O_4@SiO_2 NPs (Figs. S2–S3), all of the three materials display characteristic Fe–O absorption bands at approximately 580 and 1700 cm^{-1}. The successful thiol functionalization of Fe_3O_4–RSH NPs was further confirmed by Raman spectroscopy. As illustrated in Fig. 1b, a pronounced Raman band at 1095 cm^{-1} corresponds to the C–S stretching vibration of Fe_3O_4–RSH NPs.[36] Additional bands at 559 and 358 cm^{-1} are attributed to Fe–O bond vibrations of Fe_3O_4–RSH NPs and Si–O bond vibrations of the surface-modifying agent 3-MPTMS, respectively. Fig. 1c displays the XRD patterns of Fe_3O_4–RSH NPs. Diffraction peaks are observed at approximately 30.2°, 35.4°, 43.1°, 53.4°, 57.1°, and 62.6°,

corresponding to the (220), (311), (400), (422), (511), and (440) crystallographic planes of Fe_3O_4 NPs, consistent with the standard JCPDS card 99-0073.[37] Compared to Fe_3O_4 NPs and Fe_3O_4@SiO_2, the results indicate that Fe_3O_4-RSH NPs retained their typical cubic spinel structure throughout the modification process. The XPS data of prepared Fe_3O_4-RSH NPs are shown in Fig. 1d. The high-resolution Fe XPS spectrum of Fe_3O_4-RSH NPs (Fig. 1e) shows two peaks at 723.81 and 710.44 eV, corresponding to Fe $2p_{1/2}$ and Fe $2p_{3/2}$, respectively. The peaks observed at 530 eV and 531.75 eV in the high-resolution O XPS spectrum (Fig. 1f) correspond to signals from the Fe-O and O-H bonds in the material. Compared to the precursor materials (Figs. S2-S3), the high-resolution XPS spectra of Fe and O elements for all materials were essentially consistent. However, Fe_3O_4-RSH NPs exhibited a peak at 163.3 eV in the high-resolution S XPS spectrum (Fig. 1g), corresponding to the sulfur groups on the material's surface, confirming the successful introduction and modification of the thiol group.[38]

The morphology and size of the Cu NPs, CuS NPs, and CuO NPs were characterized. TEM images (Figs. S4 a, c, e) show that Cu NPs, CuS NPs, and CuO NPs exhibit near-spherical shapes and are randomly dispersed in ultrapure water. The average particle sizes were 4.18 ± 0.68 nm, 4.95 ± 0.82 nm, and 5.01 ± 0.81 nm, respectively (Figs. S4 b, d, f). The particle sizes were uniformly distributed around 5 nm, thereby eliminating the influence of varying particle sizes on the results of subsequent filtration experiments.

Feasibility for Cu NPs separation by Fe_3O_4-RSH NPs - modified membrane. Fig. S5 presents SEM images of commercial MCE membranes (nominal pore size: 0.22 μm) following modification with progressively increasing loadings of Fe_3O_4–RSH NPs. During vacuum filtration, the nanoparticles are deposited onto the cellulose scaffold. As the deposition mass of the modifier increases, the surface roughness of the film also increases accordingly, with Fe_3O_4-RSH NPs increasingly covering the fiber network (Fig. S5a–g). At the highest nanoparticle loading (Fig. S5g), a dense and continuous selective layer is formed, which is expected to enhance the selective retention of target nanoparticles. During membrane modification, the surface loading efficiency calculation formula for thiol-modified Fe_3O_4-RSH NPs on filter membranes is:

$$R_{MNPs}(\%) = \frac{W\text{-}W_0}{M} \quad (2)$$

where W is the mass of the modified and dried membrane, W_0 is the mass of the unmodified membrane, and M is the mass of the modifier dispersed in distilled water.

As shown in Table. S1, the surface loading efficiency of the modified material on the membrane improved with increasing nanoparticle loading, rising from 80.00% to 99.52%.[39]

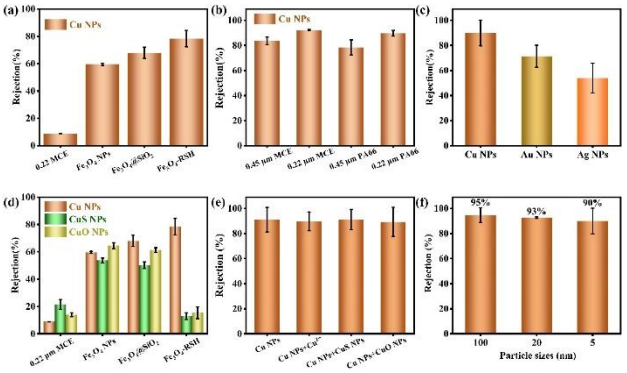

Fig. 2 (a) Retention capacity of modified membranes made from different materials for Cu NPs. (b) Retention capacity of modified membranes on different substrates for Cu NPs. (c) Rejection efficiency of 5 nm nanoparticles (Cu NPs, Au NPs, and Ag NPs). (d) Retention capacity of modified membranes made from different materials for multiple types of Cu NPs. (e) Rejection of Cu NPs in mixtures with 5 ng mL^{-1} Cu^{2+}, CuS NPs, and CuO NPs. (f) Rejection of Cu NPs of 5, 20, and 100 nm sizes.

As illustrated in Scheme. 1, a disposable syringe-filter assembly was used for the rapid separation of Cu NPs. As shown in Fig. 2a, compared to the unmodified membrane, Fe_3O_4 NPs and Fe_3O_4@SiO_2 NPs modified membrane, the Fe_3O_4–RSH NPs modified filters exhibit significantly higher rejection of Cu NPs (>80%). The membranes with different pore sizes (0.22 μm and 0.45 μm) and compositions (MCE and nylon) were uniformly functionalized with Fe_3O_4–RSH nanoparticles and systematically characterized. As shown in Fig. 2b, the 0.22 μm MCE membrane exhibited the highest Cu NP rejection rate of 90%, indicating excellent separation performance. Subsequently, three nanomaterials (Au NPs, Ag NPs, and Cu NPs) with identical particle sizes and concentrations were filtered to evaluate the retention efficiency of the modified membrane. As shown in Fig. 2c, the membrane exhibited the highest retention efficiency for Cu NPs, indicating its superior selectivity toward copper nanoparticles. The selectivity of the variously modified membranes was evaluated for the separation of Cu NPs, CuS NPs, and CuO NPs. As shown in Fig. 2d, the Fe_3O_4–RSH NPs–modified membrane exhibited high selectivity for Cu NPs in comparison to similarly sized CuS and CuO NPs. The capacity of the Fe_3O_4–RSH NPs–modified membrane to discriminate Cu NPs exceeded that of membranes modified with other materials. To evaluate the effect of other copper species on the membrane's separation performance toward Cu NPs, additional experiments were carried out in which 5 ng mL^{-1} Cu NPs were individually mixed with equal concentrations of Cu^{2+}, CuO NPs, and CuS NPs. As shown in Fig. 2e, the retention rate of Cu NPs remained unchanged in the presence of these copper species, indicating that the filter membrane exhibits excellent selectivity toward Cu NPs. To assess the size-dependent separation performance of the modified filter membrane, Cu NPs with diameters of 5, 20, and 100 nm were filtered. As shown in Fig. 2f, the membrane exhibited

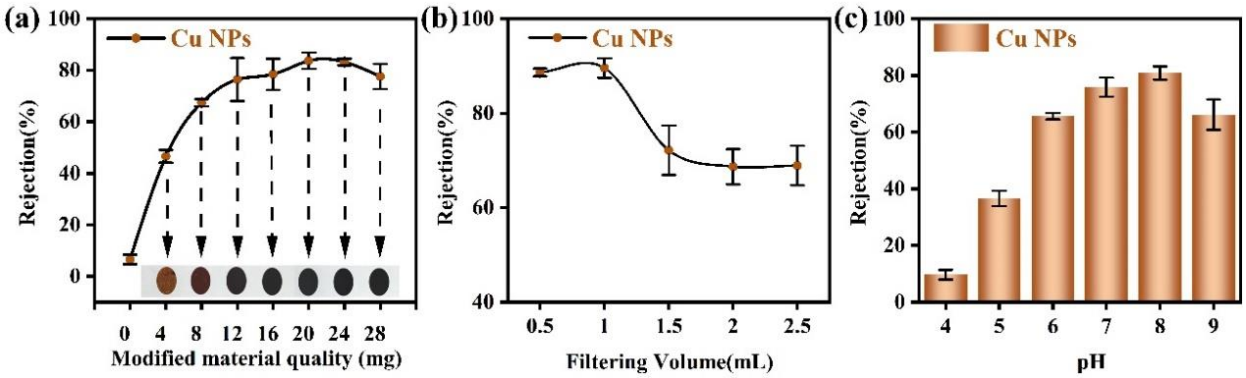

Fig. 3 (a) Effect of modified material dosage on Cu NP retention rate. (b) Effect of filtrate volume on Cu NP retention rate. (c) Effect of pH on Cu NP retention rate.

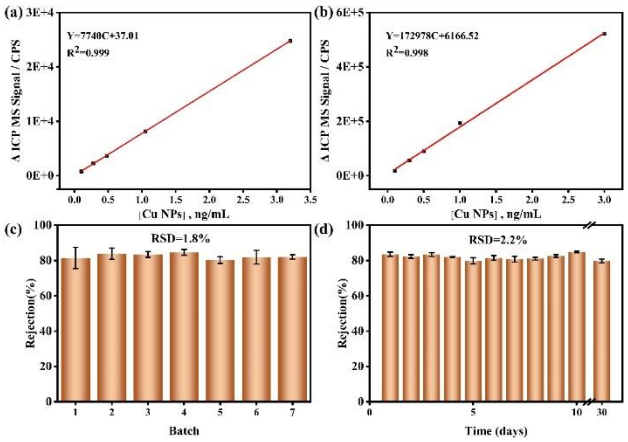

Fig. 4 Linear relationship between Cu NP concentration and ICP-MS signal intensity (b) before and (a) after extraction. (c) Inter-batch stability and (d) time stability of modified filter membranes.

high filtration efficiency (>90%) for all tested particle sizes, with the efficiency gradually increasing as particle size increased.

Optimization of experiment condition. To achieve optimal filtration and separation performance of the Fe_3O_4-RSH NPs - modified filtration, key experimental parameters were systematically optimized. As shown in Fig. 3a, Cu NPs retention increased progressively with Fe_3O_4–RSH NPs loading, reaching a maximum at 20 mg. As shown in Fig. 3b, filtration efficiency was evaluated using different volumes of Cu NPs solution, with the highest retention observed at 1 mL. Further evaluation across a pH range of 4–9 revealed that the Fe_3O_4–RSH NPs-modified membrane achieved maximum and highly reproducible rejection of Cu NPs at pH 8 (Fig. 3c), consistent with the typical pH of environmental waters.

Analytical performance. Under optimized conditions, the analytical performance for Cu NPs was evaluated. As shown in Fig. 4a, a strong linear correlation (Y = 175,538 C + 30.03) was observed, with the LOD calculated as 3 σ / k (where σ represents the standard deviation of 11 blank measurements and k denotes the slope of the calibration curve) to be 2.2 pg mL^{-1} for Cu NPs. Compared with direct analysis without membrane extraction (Fig. 4b), the use of the Fe_3O_4-RSH NPs modified membrane followed by elution with HNO_3 achieved a 23-fold preconcentration factor. Subsequently, seven batches of Fe_3O_4-RSH NPs - modified filtration were fabricated to evaluate the reproducibility of Cu NPs filtration. As shown in Fig. 4c, the relative standard deviation (RSD) was 1.8%, indicating excellent reproducibility. Membranes prepared using the same modification strategy were further tested for Cu NP filtration over a period of 7 to 30 days. As presented in Fig. 4d, the results showed an RSD of 2.2%, demonstrating the long-term storage stability of the modified membranes.

The reusability of the modified membrane was also investigated by performing multiple filtration cycles using the Fe_3O_4–SH functionalized membrane. As shown in Fig. S6a, the retention efficiency for Cu NPs remained around 90% during the first three consecutive filtration cycles, demonstrating good initial stability. However, after cleaning the membrane with 2% HNO_3 (Fig. S6b) and distilled water assisted by ultrasonication (Fig. S6c), followed by re-modification, a pronounced decline in filtration efficiency was observed. This reduction was likely caused by damage to the fiber structure of the commercial MCE membrane, which substantially impaired its overall filtration performance.

To evaluate the selectivity of the method, the recoveries of 1 ng mL^{-1} Cu NPs were measured in the presence of a 100-fold excess (100 ng mL^{-1}) of common cations and anions in natural waters, including Na^+, K^+, Mg^{2+}, Ca^{2+}, Al^{3+}, Mn^{2+}, Fe^{3+}, Ni^{2+}, Zn^{2+}, and SO_4^{2-}. All tested ions produced recoveries between 93 and 101% (Table 1), indicating negligible interference and confirming the suitability of the method for direct analysis of environmental samples.

Table 1. Interference study of common ions

Interference	[M] (ng mL^{-1})	[M]/ Cu NPs (ng mL^{-1})	Recovery (%)
Na^{+}	100	1	97
Mg^{2+}	100	1	98
Al^{3+}	100	1	97
K^{+}	100	1	101
Ca^{2+}	100	1	94
Mn^{2+}	100	1	98
Fe^{3+}	100	1	96
Ni^{+}	100	1	94
Zn^{2+}	100	1	101
SO_4^{2-}	100	1	93

Table 2. The results of Cu NPs analysis in the Chengdu River

Sample	Added (ng mL^{-1})	Found (ng mL^{-1})	RSD (%)	Recovery (%)
Jiang'an Lake	0	0.11	-	-
	1.00	1.12±0.03	3.9	101
Luhu Lake	0	0.13	-	-
	1.00	1.10±0.03	1.8	97
Yixin Lake	0	0.13	-	-
	1.00	1.06±0.01	0.8	93
South Lake	0	0.08	-	-
	1.00	1.11±0.02	2.3	103

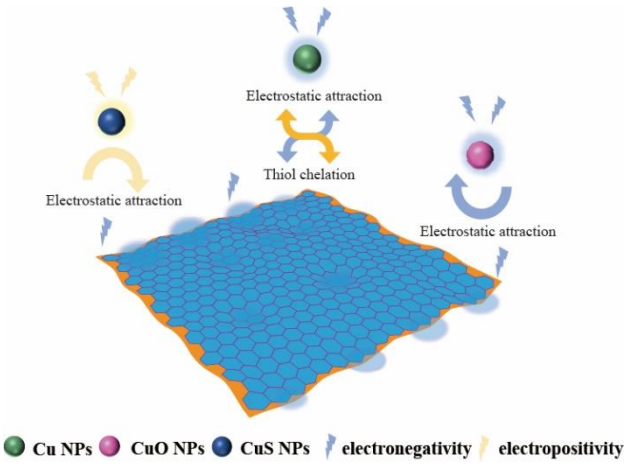

Fig. 5 The mechanism of filtering different copper-based nanoparticles by Fe_3O_4-RSH NPs modified filtration membrane.

Mechanism of selective filtration by Fe_3O_4-RSH NPs - modified membrane. The selective filtration of Cu NPs from mixtures containing CuS and CuO NPs is governed not only by the membrane's pore size and steric effects but also by its material composition, surface charge, and the functional groups and charge properties of the nanoparticles.[40] Owing to the ultrafine size (≈5 nm) of all three copper-based nanoparticles, their separation is determined primarily by the surface charge characteristics of the membrane rather than by size exclusion. The commercially available MCE membrane is electrically neutral, resulting in a negligible Donnan effect and, consequently, poor selectivity among Cu, CuO, and CuS NPs.[41] In contrast, modification with Fe_3O_4–RSH NPs confers a positive surface charge (ζ-potential ≈ +7.733 mV), which induces strong Donnan repulsion against positively charged Cu NPs and CuO NPs, thereby enhancing rejection efficiency (Fig. S7a).[42] In addition, the thiol groups provided by Fe_3O_4–RSH NPs form stable Cu–S coordination complexes. Post-filtration XPS analysis revealed a Cu $2p_{3/2}$ peak at 939.2 eV, indicative of Cu–S bonding, thereby confirming the selective chelation of Cu NPs (Fig, S7b–c). Collectively, these results demonstrate that the modified membrane can selectively retain Cu NPs from mixed suspensions of copper-based nanoparticles under environmentally relevant conditions (Fig. 5).

Real sample analysis. Driven by their widespread use in industry, agriculture, and consumer products, Cu NPs have dispersed across all environmental compartments, making their reliable quantification essential for accurate exposure assessment and ecological risk evaluation.[43] In this study, Cu NPs were measured in water samples collected from four different locations along the Chengdu River, with concentrations ranging from 0.09 to 0.13 ng mL^{-1}. The accuracy of the method was evaluated through spiking experiments. As summarized in Table 2, recoveries ranged from 93% to 103%, with RSDs consistently below 5%. These results demonstrate that the developed method is effective for the filtration and selective separation of Cu NPs from environmental water samples.

CONCLUSION

In this study, we developed a simple and cost-effective approach to fabricate a functionalized filtration membrane by immobilizing Fe_3O_4–RSH NPs onto MCE membranes via vacuum filtration. The resulting membrane exhibited outstanding selectivity for Cu NPs, achieving over 90% retention while maintaining excellent stability. It effectively separated Cu NPs from other copper-based nanoparticles of similar size and properties in mixed samples. This method enabled rapid preconcentration of Cu NPs, providing an enrichment factor of ~23 and low detection limits when coupled with ICP-MS analysis. Its successful application to detect and isolate Cu NPs from river water samples in Chengdu demonstrates its practical utility for environmental monitoring. Notably, this work represents the first use of a thiol-modified Fe_3O_4-based membrane for selective Cu NPs separation, offering a reliable, rapid, and low-cost pretreatment strategy for enriching and analyzing trace nanoparticles in complex environmental matrices.

Looking ahead, this filtration strategy shows great potential for advancing nanoparticle separation technologies. Its capability to efficiently isolate nanoparticles with similar elemental compositions and sizes paves the way for broader applications,

including the monitoring of diverse metal and engineered nanoparticles in environmental systems. Future research could focus on enhancing membrane scalability and developing more versatile filtration platforms for multi-metal nanoparticle separation. Moreover, integrating this method with portable, on-site detection devices may revolutionize environmental monitoring by enabling real-time, low-cost analysis in remote or resource-limited areas. Beyond environmental applications, this approach could be extended to industrial wastewater treatment, water purification, and biomedical fields, where precise nanoparticle separation is of critical importance.

ASSOCIATED CONTENT

The supporting information (Figs. S1−S7 and Table S1) is available at https://www.at-spectrosc.com.

AUTHOR INFORMATION

Ke Huang is a professor at the Sichuan Normal University. He received his BSc degree in 2010 from the College of Chemistry, Sichuan University, Ph.D. degree in 2015 in analytical chemistry from the College of Chemistry, Sichuan University. He began his independent career in the College of Chemistry and Material Science, Sichuan Normal University. His current research interest is atomic spectroscopy bioanalysis. Ke Huang is the author or co-author of over 100 articles published in peer-reviewed scientific journals.

Corresponding Author

*K. Huang

Email address: huangke@sicnu.edu.cn

Notes

The authors declare no competing financial interest.

ACKNOWLEGMENTS

This work was supported by National Natural Science Foundation of China (21605108), Sichuan Science and Technology Program (2023NSFSC1090), Open Research Fund of Fire Protection and Retardant Technology, Ministry of Emergency Management (FHZR2023KFMS_05), Opening Foundation from Key Lab of Process Analysis and Control of Sichuan Universities (GCFX2024004) and Foundation of Sichuan Normal University (SYJS2023008 and ZZYQ2023004).

REFERENCES

1. A. D. Kute, R. P. Gaikwad, I. R. Warkad, and M. B. Gawande, *Green Chem.*, 2022, **24**. 3502-3573. https://doi.org/10.1039/D1GC04400A
2. M. B. Gawande, A. Goswami, F. X. Felpin, T. Asefa, X. X. Huang, R. Silva, X. X. Zou, R. Zboril, and R. S. Varma, *Chem. Rev.*, 2016, **116**. 3722-3811. https://doi.org/10.1021/acs.chemrev.5b00482
3. Z.-X. Chen, Y.-J. Song, R.-Z. Li, S.-J. Guo, L. Shi, Z.-R. Yang, X.-M. Xue, and T. Zhang, *Coord. Chem. Rev.*, 2025, **529**. 216455. https://doi.org/10.1016/j.ccr.2025.216455
4. M. L. Ermini and V. Voliani, *ACS Nano*, 2021, **15**. 6008-6029. https://doi.org/10.1021/acsnano.0c10756
5. W. Zhang, V. Munyaneza, S. Kant, S. Wang, X. Wang, H. Cai, C. Wang, L. Shi, S. Wang, F. Xu, and G. Ding, *J. Hazard. Mater.*, 2024, **480**. 136186. https://doi.org/10.1016/j.jhazmat.2024.136186
6. N. Wang, B. Wang, and X. Zhang, *Chem. Eng. J.*, 2024, **498**. 155441. https://doi.org/10.1016/j.cej.2024.155441
7. Q.-G. Tan, W. Zhou, and W.-X. Wang, *Environ. Sci. Technol.*, 2018, **52**. 484-492. https://doi.org/10.1021/acs.est.7b04906
8. H. Liu, W. Lai, X. Liu, H. Yang, Y. Fang, L. Tian, K. Li, H. Nie, W. Zhang, Y. Shi, L. Bian, S. Ding, J. Yan, B. Lin, and Z. Xi, *J. Hazard. Mater.*, 2021, **401**. 123349. https://doi.org/10.1016/j.jhazmat.2020.123349
9. T. Ghomian and J. Hihath, *IEEE Trans. Biomed. Eng.*, 2023, **70**. 27-41. 10.1109/TBME.2022.3183167
10. Q.-c. Li, Y.-j. Lai, S.-j. Yu, P. Li, X.-x. Zhou, L.-j. Dong, X. Liu, Z.-w. Yao, and J.-f. Liu, *Anal. Chem.*, 2021, **93**. 4559-4566. https://doi.org/10.1021/acs.analchem.0c04996
11. U. Shashvatt, F. Amurrio, and L. Blaney, *Environ. Sci. Technol.*, 2022, **56**. 13945-13953. https://doi.org/10.1021/acs.est.2c02153
12. M. S. Jagirani and M. Soylak, *Microchem. J.*, 2020, **159**. 105436. https://doi.org/10.1016/j.microc.2020.105436
13. M. Soylak and M. Do°an, *Anal. Lett.*, 1996, **29**. 635-643. https://doi.org/10.1080/00032719608000426
14. L. Liu, B. He, Q. Liu, Z. Yun, X. Yan, Y. Long, and G. Jiang, *Angew. Chem. Int. Ed.*, 2014, **53**. 14476-14479. https://doi.org/10.1002/anie.201408927
15. X.-x. Zhou, J.-f. Liu, and G.-b. Jiang, *Environ. Sci. Technol.*, 2017, **51**. 3892-3901. https://doi.org/10.1021/acs.est.6b05539
16. J. Navratilova, A. Praetorius, A. Gondikas, W. Fabienke, F. Von der Kammer, and T. Hofmann, in *Int. J. Environ. Res. Public Health*. 2015, **12**. 15756-15768. https://doi.org/10.3390/ijerph121215020
17. H.-L. Huang, *J. Mol. Liq.*, 2017, **230**. 24-27. https://doi.org/10.1016/j.molliq.2016.12.112
18. H.-L. Huang, H. Wang, G.-T. Wei, I. W. Sun, J.-F. Huang, and Y.-W. Yang, *Environ. Sci. Technol.*, 2006, **40**. 4761-4764. https://doi.org/10.1021/es060034s
19. X. Chen, H. Kelin, Z. Jinrong, Y. Xin, Z. Mei, H. Ke, and Y. and Pan, *Appl. Spectrosc. Rev.*, 2024, **59**. 315-339. https://doi.org/10.1080/05704928.2022.2134145
20. Y. Liu, J. Zhu, M. Chi, G. V. Eygen, K. Guan, and H. Matsuyama, *Chem. Eng. J.*, 2025, **506**. 160132. https://doi.org/10.1016/j.cej.2025.160132

21. X. Liu, J. Zhang, H. Wu, F. Li, Z. Liu, Y. Ma, and J. Meng, *Desalination*, 2025, **613**. 119067. https://doi.org/10.1016/j.desal.2025.119067
22. J. Yang, F. Sun, L. Zhao, D. Y. Xing, W. Dong, and Z. Dong, *J. Membr. Sci.*, 2020, **603**. 117767. https://doi.org/10.1016/j.memsci.2019.117767
23. G. Yi, L. Du, G. Wei, H. Zhang, H. Yu, X. Quan, and S. Chen, *J. Membr. Sci.*, 2022, **658**. 120719. https://doi.org/10.1016/j.memsci.2022.120719
24. M. Ouda, R. P. Pandey, and S. W. Hasan, *Desalination*, 2024, **592**. 118093. https://doi.org/10.1016/j.desal.2024.118093
25. K. Wang, X. Wang, B. Januszewski, Y. Liu, D. Li, R. Fu, M. Elimelech, and X. Huang, *Chem. Soc. Rev.*, 2022, **51**. 672-719. https://doi.org/10.1039/D0CS01599G
26. W. Yu, Y. Liu, Y. Xu, R. Li, J. Chen, B.-Q. Liao, L. Shen, and H. Lin, *J. Membr. Sci.*, 2019, **581**. 401-412. https://doi.org/10.1016/j.memsci.2019.03.083
27. F. Almomani, R. Bhosale, M. Khraisheh, A. kumar, and T. Almomani, *Appl. Surf. Sci.*, 2020, **506**. 144924. https://doi.org/10.1016/j.apsusc.2019.144924
28. Z. Qi, T. P. Joshi, R. Liu, H. Liu, and J. Qu, *J. Hazard. Mater.*, 2017, **329**. 193-204. https://doi.org/10.1016/j.jhazmat.2017.01.007
29. M. I. A. Abdel Maksoud, A. M. Elgarahy, C. Farrell, A. a. H. Al-Muhtaseb, D. W. Rooney, and A. I. Osman, *Coord. Chem. Rev.*, 2020, **403**. 213096. https://doi.org/10.1016/j.ccr.2019.213096
30. S. Liu, B. Yu, S. Wang, Y. Shen, and H. Cong, *Adv. Colloid Interface Sci.*, 2020, **281**. 102165. https://doi.org/10.1016/j.cis.2020.102165
31. G. Li, M. Liu, Z. Zhang, C. Geng, Z. Wu, and X. Zhao, *J. Colloid Interface Sci.*, 2014, **424**. 124-131. https://doi.org/10.1016/j.jcis.2014.03.026
32. Q. U. Ain, U. Rasheed, M. Yaseen, H. Zhang, and Z. Tong, *J. Hazard. Mater.*, 2020, **397**. 122758. https://doi.org/10.1016/j.jhazmat.2020.122758
33. H. Qiu, S. Chen, J. Zhang, and Q. Zhang, *J. Hazard. Mater.*, 2025, **494**. 138576. https://doi.org/10.1016/j.jhazmat.2025.138576
34. J. Ge, Y. Hu, M. Biasini, W. P. Beyermann, and Y. Yin, *Angew. Chem. Int. Ed.*, 2007, **46**. 4342-4345. https://doi.org/10.1002/anie.200700197
35. M. S. T. Dehaghani, Z. Esfandiari, and M. Khodadadi, *Food Chem.*, 2025, **481**. 143939. https://doi.org/10.1016/j.foodchem.2025.143939
36. Y. Y. Wang, H. Shi, Y. Gong, B. Zhang, B. Zhao, R. Li, and S. B. Cronin, *Langmuir*, 2023, **39**. 16807-16811. https://doi.org/10.1021/acs.langmuir.3c02073
37. A. Khalid, R. M. Ahmed, M. Taha, and T. S. Soliman, *J. Alloys Compd.*, 2023, **947**. 169639. https://doi.org/10.1016/j.jallcom.2023.169639
38. Y. Pi, C. Duan, Y. Zhou, S. Sun, Z. Yin, H. Zhang, C. Liu, and Y. Zhao, *J. Hazard. Mater.*, 2022, **424**. 127577. https://doi.org/10.1016/j.jhazmat.2021.127577
39. D. Jassby, S.-R. Chae, Z. Hendren, and M. Wiesner, *J. Colloid Interface Sci.*, 2010, **346**. 296-302. https://doi.org/10.1016/j.jcis.2010.03.029
40. Y. Wu, Y. Wang, L. Yan, K. Huang, K. Chang, and P. Chen, *Small Methods*, 2025, **9**. 2500314. https://doi.org/10.1002/smtd.202500314
41. Y. Wu, J. Liu, S. Li, R. Jian, X. Yuan, and K. Huang, *Sci. Total Environ.*, 2024, **954**. 176416. https://doi.org/10.1016/j.scitotenv.2024.176416
42. P. Aydogan Gokturk, R. Sujanani, J. Qian, Y. Wang, L. E. Katz, B. D. Freeman, and E. J. Crumlin, *Nat. Commun.*, 2022, **13**. 5880. https://doi.org/10.1038/s41467-022-33592-3
43. X. Wang and W.-X. Wang, *Environ. Sci. Technol.*, 2023, **57**. 9548-9558. https://doi.org/10.1021/acs.est.3c00864